Kinetics and Catalysis, Vol. 46, No. 6, 2005, pp. 775–788. Translated from Kinetika i Kataliz, Vol. 46, No. 6, 2005, pp. 821–834.

Effect of a Gas Discharge on the Ignition in the Hydrogen–Oxygen System

R. S. Konstantinovskii, V. M. Shibkov, and L. V. Shibkova

Faculty of Physics, Moscow State University, Vorob'evy gory, Moscow, 119899 Russia

Received June 11, 2004

Abstract—A kinetic model is constructed for ignition initiated by nonequilibrium gas-discharge plasma in the hydrogen–oxygen system. The model takes into account the effect of the electric field on the dissociation of molecules and on the buildup of active radicals, excited species, and charged species (electrons and positively and negatively charged ions). It is demonstrated by mathematical modeling that the induction period depends strongly on the reduced strength of the electric field (electron temperature). Four reduced kinetic networks are considered, and various components and reactions are shown to exert an effect on the nonthermal initiation of ignition in the H_2–O_2 system by low-temperature plasma.

The mechanism of the gas-phase oxidation of various combustible gases, including hydrocarbons and hydrogen, has been thoroughly studied (see, e.g., [1–8]), with the emphasis on their ignition mechanism. The great majority of publications in this field have dealt with factors determining the induction period preceding the ignition event. In recent decades, there has also been much literature discussing the possibility of effectively controlling combustion processes by various physical means. For example, Semenov [9] studied the broadening of the inflammability range of the hydrogen–oxygen mixture under the action of shortwave radiation or oxygen atoms. Furthermore, it has been experimentally demonstrated that, under the action of ultraviolet radiation ($\lambda \le 175$ nm), the inflammability "peninsula" broadens and shifts to lower temperatures [10]. In a number of works, it is suggested to initiate ion–molecule and ion–atom reactions using low-temperature gas-discharge plasma [11, 12]. In the same works, plasma jets and laser radiation are discussed as possible ignitors for supersonic hydrocarbon streams. Numerical analysis and experimental studies of the ignition of argon- or helium-diluted H_2–O_2, H_2–air, and CH_4–O_2 mixtures with a nanosecond high-voltage discharge at various temperatures, mixture compositions and pressures, and energies deposited in the discharge have revealed marked distinctions between the equilibrium and nonequilibrium excitations of the mixtures [13]. The effects of the initial concentration of free radicals (H and O atoms) and of the radiolysis rates of dihydrogen and dioxygen on the ignition limits of the stoichiometric hydrogen–oxygen mixture have been studied by numerical simulation [14]. The ignition temperature near the first limit appeared to be the most sensitive to the dihydrogen and dioxygen radiolysis rates. Numerical simulation predicts that singlet oxygen $O_2(a^1\Delta_g)$ will cause an increase in the hydrogen–oxygen flame velocity [15]. This result is in qualitative agreement with experimental data. Furthermore, this promoting effect is predicted to be nonlinear: doubling the amount of singlet oxygen increases the calculated flame propagation rate only by one-third. The ignition of various hydrocarbon-containing combustible mixtures by laser heating or laser-induced breakdown has been studied as a function of gas pressure and laser wavelength [16–18]. Although this laser treatment exerts a strong effect on the ignition of the mixture, it suffers from an essential drawback as applied to hypersonic ramjets: it is impossible to initiate ignition in a large volume.

A cursory survey of the literature has demonstrated that there are numerous ways of intensifying the chain combustion of hydrocarbons. However, the ignition kinetics is not completely understood even for the rather simple model hydrogen–oxygen system under low-temperature gas-discharge plasma conditions, which are established at large values of the reduced electric field. Therefore, for deeper insight into the physicochemical processes occurring in the low-temperature plasma initiation of the ignition of a combustible gas, the experimental study of the effect of a gas discharge on the ignition event should be accompanied by mathematical modeling. The study of the ignition and combustion of hydrogen-containing mixtures under low-temperature plasma conditions is of importance from various standpoints: it is necessary to carry out both fundamental research in the mechanism and kinetics of atom–molecule reactions in a strong electric field and the analysis of a variety of applied problems, including the optimization of plasma chemical processes. One practical problem is to develop the physical

0023-1584/05/4606-0775 © 2005 MAIK "Nauka/Interperiodica"

principles of the hypersonic ramjet. In order to diminish the ramjet length, it is necessary to ensure a rapid space ignition of the high-velocity hydrocarbon flow. To do this, it is necessary to minimize the induction period.

The following important questions should be answered for the successful application of gas discharges in supersonic plasma aerodynamics:

What type of gas discharge will ensure the quickest and most perfect mixing of the supersonic hydrocarbon flow with air?

Is a gas discharge capable of quickly and reliably igniting a supersonic stream of a gaseous fuel?

Is it possible to ensure, using a gas discharge, the stable and complete burning of the fuel at the minimum possible electric energy supply to the supersonic flow?

Here, using the hydrogen–oxygen system as a model, we consider the mechanism of the ignition of a gaseous fuel with nonequilibrium gas-discharge plasma. A combustible gas mixture can be ignited either by heating it to a high temperature (autoignition) or by the nonthermal buildup of free radicals and active species using an external source of energy. The main purpose of this study is to determine the mechanism that is responsible for the ignition of a gas fuel in the presence of nonequilibrium discharge plasma at a high reduced strength of the electric field. Other important tasks of this study are to evaluate the effect of discharge parameters on the ignition kinetics of the gaseous fuel and to simulate the combustion of the fuel under the action of a discharge.

EXPERIMENTAL

In our laboratory, we initiate ignition with dc discharges (either longitudinal or transverse to the supersonic flow), periodic pulsed discharges [19], radio-frequency electrode discharges, and space [20] and surface [21] microwave discharges. Initially, the effect of low-temperature plasma on the combustion kinetics of a gaseous fuel was experimentally studied for a supersonic propane–butane–air flow with a Mach number of $M = 2$.

Our experimental setup consists of a cylindrical vacuum chamber with an inner diameter of 1 m and a length of 3 m, a high-pressure air receiver, a high-pressure propane–butane receiver, a system for mixing the propane–butane mixture with air, a system for producing a supersonic propane–butane–air flow, an aerodynamic channel, a discharge section, three plasma generators, a pulsed high-voltage power supply, a synchronization system, and a diagnostic system. The air flow rate can be varied between 25 and 100 g/s; the propane–butane flow rate, between 1 and 8 g/s. The basic part of this setup is the vacuum chamber, which serves to produce a supersonic flow and is a reservoir for the exhaust gases and combustion products. The vacuum system allows operation in a wide pressure range of $P = 10^2$–10^5 Pa. We used three types of gas discharge for ignition: unconfined localized microwave discharge [22], surface microwave discharge [23], and pulsed transverse electrode discharge [24]. The ignition of the supersonic stream was detected as a glow in the aerodynamic channel downstream of the discharge section. No glow was observed when a gas discharge was generated in an air flow, when it was generated in a supersonic propane–butane–air flow but its parameters (pulse duration, discharge current, electric field strength in the plasma, and the electric power deposited in the discharge) were inappropriate for ignition, or when the mixture was far from stoichiometric. Induction time was simultaneously derived from different measurements: (1) the minimum microwave pulse duration resulting in a glowing flame in the aerodynamic channel downstream of the discharge section; (2) the time taken by the intensity of the molecular band of the excited CH^* radical (the (0;0) band due to the $A^2\Delta \longrightarrow X^2\pi$ transition), with an edge wavelength of $\lambda = 431.5$ nm, to achieve the maximum growth rate; (3) the time taken by the signal from the double probe to achieve the maximum growth rate; and (4) the time taken by the current through the plane capacitor at the outlet of the aerodynamic channel to achieve the maximum growth rate. The ignition of the supersonic flow was also detected as an increasing output signal from an acoustic noise meter. The ignition of the hydrocarbon fuel in the supersonic flow several times raised the noise level measured by the microphone.

Different discharges afford different degrees of gas ionization at the same specific power deposited. The electric energy supplied is nonuniformly distributed among the internal degrees of freedom of the molecular gas. This distribution depends strongly on the reduced strength of the electric field, which, in turn, is determined by the electrodynamics of the discharge. Experiments have demonstrated that a periodic pulsed electrode discharge causes ignition only at a pulse duration of $\tau > 150$ μs. The ignition of a supersonic propane–butane–air flow with an unconfined localized microwave discharge is possible at $\tau \approx 25$ μs, and the ignition of the same mixture with a surface microwave discharge takes place almost immediately after the microwave generator is turned on. At high reduced field strengths ($E/n \geq 10^{15}$ V cm^2), more than 50% of the power deposited in the discharge is spent for the excitation, dissociation, and electron-impact ionization of molecules followed by the generation of reactive free radicals [25]. Since the self-sustained microwave discharge takes place at high reduced field strengths [20, 26], it produces more active species than the electrode discharge. This must exert a strong effect on the kinetics of the processes involving active radicals to shorten the induction period.

Our results lend credence to the finding that, at a high reduced strength of the electric field, the gas in microwave plasma is rapidly heated at a rate of $dT_g/dt = 10^7$–10^8 K/s and its molecules achieve a high degree of

dissociation ($\delta \approx 50\%$) [27–30]. This favors a quick ignition of the fuel. Therefore, we consider it necessary to thoroughly study the effects of the charged and active species rapidly generated in the discharge on the ignition delay time and hydrocarbon combustion efficiency.

MATHEMATICAL MODEL

A mathematical model was constructed for a motionless hydrogen–oxygen mixture. In order to determine the roles of various reaction channels in the ignition of the combustible mixture, we developed a kinetic model including 29 components and 241 forward and back reactions (Tables 1–4). We took into consideration the neutral unexcited species H_2, O_2, H, O, OH^*, HO_2^*, H_2O_2, H_2O, and O_3; the electronically excited oxygen molecules $O_2(a)$ and $O_2(b)$; the positively charged ions O^+, O_2^+, O_4^+, H^+, H_2^+, H_3^+, H_5^+, OH^+, H_2O^+, H_3O^+, and $O_3H_2^+$; the negatively charged ions O^-, O_2^-, O_3^-, O_4^-, H^-, and OH^-; and electrons (e). Tables 1 and 2 list the reactions included in the model as well as the coefficients ($A^\pm$, $m^\pm$, and $E^\pm$) determining the temperature-dependent rate constants of the forward (+) and back (–) reactions $k^\pm = A^\pm T^{m^\pm} \exp(E^\pm/T)$. Table 3 lists the rate constants $k^+ = A^+ T_e^{m_e^+} \exp(E_e^+/T_e)$ depending on the electrode temperature T_e, and Table 4 lists the rate constants $k^+ = A^+ \exp(E_\theta^+/\theta)$ depending on the reduced field strength θ. The rate constants were derived from data reported in earlier works [7, 31–41]. The constants $k^\pm$ have dimensions of $(\mathrm{cm}^3\ \mathrm{mol}^{-1})^{m_i^\pm - 1}\ \mathrm{s}^{-1}$, $E^\pm$ and T have dimensions of K, E_e^+ and T_e have dimensions of eV, and E_θ^+ and θ have dimensions of 10^{-16} V cm^2. If the necessary data for a back reaction were not found in the literature, the rate constant of this reaction was calculated as $k_i^- = k_i^+ (RT)^{\Delta m_i}/K_{e,i}$, $R\ln K_{e,i} \Delta\Phi_i^0(T) - \Delta H_i^0(0)/T$, where R is the universal gas constant, Δm_i is the change in the number of reacting molecules, and $\Delta\Phi_i^0(T)$ and $\Delta H_i^0(0)$ are the changes in the reduced Gibbs energy and enthalpy at $T = 0$ K for the ith reaction. The $\Delta H_i^0(0)$ values and polynomials for calculating $\Delta\Phi_i^0(T)$ can be found in [42]. In Tables 1–4, we use the following contracted notation: 2.1(15) should be understood as 2.1×10^{15}, $O_2(a) = O_2(a^1\Delta_g)$, and $O_2(b) = O_2(b^1\Sigma_g^+)$.

The model of the ignition of the hydrogen–oxygen mixture is based on a set of equations describing the oxidation processes in this mixture. This set of equations includes an energy equation, a particle density (concentration) equation, and a state equation:

$$\frac{dH}{dt} = 0, \quad H = N\sum_{i=1}^{M_1}\gamma_i\left(h_{0,i}[T_0] + \int_{T_0}^{T} C_{P,i}\,dT\right),$$

$$\frac{d\gamma_i}{dt} = G_i - \gamma_i\sum_{k=1}^{M_1} G_k,$$

$$G_i = \sum_{q=1}^{M_2}\frac{\alpha_{iq}^- - \alpha_{iq}^+}{N}[R_q^+ - R_q^-],$$

$$R_q^\pm = k_q^\pm\prod_{j=1}^{n_q^\pm}(N\gamma_{n_{jq}^\pm})^{\alpha_{jq}^\pm}, \quad \frac{dN}{dt} = N\sum_{k=1}^{M_1} G_k.$$

Here, γ_i is the mole fraction of the ith component, N is the total concentration (mol/cm^3), $C_{P,i}$ is the molar heat capacity of the ith component at a constant pressure, $h_{0,i}[T_0]$ is the enthalpy of formation of the ith component at $T_0 = 298$ K, M_1 is the total number of components, $k_q^\pm$ is the constant of a reaction involving the ith component, M_2 is the total number of such reactions, and α_{iq}^+ and α_{iq}^- are stoichiometric coefficients.

RESULTS AND DISCUSSION

For a gas-discharge ignition of fuel in a hypersonic ramjet, a large space discharge should be generated in the combustor. The microwave discharge is ideally suited for this purpose: it can produce plasma of volume 10^1–10^5 cm^3 [21], depending on experimental conditions. In this case, when constructing a mathematical model in the first approximation, one can neglect the concentration and temperature gradients in the space discharge plasma. Therefore, taking into account the effect of the low-temperature plasma on the ignition of the hydrogen–oxygen mixture in the one-dimensional approximation seems to be an appropriate first step in the elucidation of the mechanism of this process under homogeneous gas discharge conditions, although this approximation may be rough.

Initially, we simulated the autoignition process. Calculations were carried out on the basis of a kinetic network including 9 components and 60 reactions (Table 1) for various temperatures T_0 and mixture compositions ϕ. The quantity $\phi = (\gamma_{H_2}/\gamma_{O_2})/(\gamma_{H_2}/\gamma_{O_2})_{st}$ is the ratio of the mole fraction of hydrogen in a given mixture to the mole fraction of hydrogen in the stoichiometric mixture. The data referring to $T_0 = 900$ K, $P_0 = 0.1$ MPa, and $\phi = 1$ are presented in Fig. 1. At the early stages of the process ($t = 0$–1 ms), when the gas temperature is

Table 1. Reaction rate constants depending on gas temperature T, $k^{\pm} = A^{\pm}T^{m^{\pm}}\exp(E^{\pm}/T)$

No.	Reaction	$A^{\pm}$	$m^{\pm}$	$E^{\pm}$	A^{-}	m^{-}	E^{-}	Reference
1	$H_2O + M = H + OH^{\cdot} + M$	1(24)	–2.2	–59000	2.2(22)	–2	0	[7]
2	$H_2 + M = 2H + M$	2.2(14)	0	–48300	9(17)	–1	0	″
3	$O_2 + M = 2O + M$	2.6(18)	0	–59580	1.1(14)	–1	900	″
4	$OH^{\cdot} + M = H + O + M$	8.5(18)	–1	–50830	7.1(18)	–1	0	″
5	$O + H_2O = 2OH^{\cdot}$	5.8(13)	0	–9059	5.3(12)	0	–503	″
6	$H_2 + O_2 = 2OH^{\cdot}$	1.7(15)	0	–24200	1.7(13)	0	–24100	″
7	$HO_2^{\cdot} + M = H + O_2 + M$	2.1(15)	0	–23000	1.5(15)	0	500	″
8	$2OH^{\cdot} = H + HO_2^{\cdot}$	1.2(13)	0	–20200	2.5(14)	0	–950	″
9	$H_2O_2 + M = 2OH^{\cdot} + M$	1.2(17)	0	–22900	9.1(14)	0	2650	″
10	$2HO_2^{\cdot} = O_2 + H_2O_2$	1.8(13)	0	–500	3(1)3	0	–21600	″
11	$O_3 + M = O + O_2 + M$	4(14)	0	–11400	6.9(12)	0	1050	″
12	$O + O_3 = 2O_2$	1.1(13)	0	–2300	1.2(13)	0	–50500	″
13	$HO_2^{\cdot} + O_3 = 2O_2 + OH^{\cdot}$	2(10)	0	–1000	k_{13}^{-}			″
14	$O + H_2 = H + OH^{\cdot}$	1.8(10)	1	–4480	8.3(9)	1	–3500	″
15	$O + H_2O = H + HO_2^{\cdot}$	4.8(11)	0.37	–28743	1(13)	0	–540	″
16	$O_2 + H_2O = OH^{\cdot} + HO_2^{\cdot}$	1.5(15)	0.5	–36600	3(14)	0	0	″
17	$OH^{\cdot} + H_2O = H_2 + HO_2^{\cdot}$	7.2(9)	0.43	–36100	6.5(11)	0	–9400	″
18	$OH^{\cdot} + HO_2^{\cdot} = O + H_2O_2$	5.2(10)	0.5	–10600	2(13)	0	–2950	″
19	$O_2 + H_2O = O + H_2O_2$	3.4(15)	0.5	–44800	8.4(11)	0	–2130	″
20	$H + O_3 = O_2 + OH^{\cdot}$	2.3(11)	0.75	0	4.4(7)	1.44	–38600	″
21	$H_2 + O_3 = OH^{\cdot} + HO_2^{\cdot}$	6(10)	0	–10000	k_{21}^{-}			″
22	$H + O_2 = O + OH^{\cdot}$	2.2(14)	0	–8455	1.3(13)		–350	″
23	$H + H_2O = H_2 + OH^{\cdot}$	8.4(13)	0	–10116	2(13)		–2600	″
24	$H_2 + O_2 = H + HO_2^{\cdot}$	1.9(13)	0	–24100	1.3(13)		0	″
25	$O_2 + OH^{\cdot} = O + HO_2^{\cdot}$	1.3(13)	0	–28200	5(13)		–500	″
26	$H + H_2O_2 = H_2 + HO_2^{\cdot}$	1.7(12)	0	–1900	6(11)		–9300	″
27	$H + H_2O_2 = OH^{\cdot} + H_2O$	5(14)	0	–5000	2.4(14)		–40500	″
28	$H_2O + HO_2^{\cdot} = OH^{\cdot} + H_2O_2$	1.8(13)	0	–15100	1(13)		–910	″
29	$OH^{\cdot} + O_3 = O_2 + HO_2^{\cdot}$	9.6(11)	0	–1000	9(8)		0	″
30	$O + 2O_2 = O_2 + O_3$	3.1(17)	–1.25	0	1(15)	0	–11400	[32]

Table 2. Reaction rate constants depending on gas temperature T, $k = AT^m\exp(E/T)$

No.	Reaction	A^+	m^+	E^+	Reference
31	$2O + O_2 = O_2 + O_2(a)$	8.9(16)	–0.63	0	[32]
32	$2O + O_2 = O_2 + O_2(b)$	8.9(16)	–0.63	0	″
33	$HO_2^{\cdot} + M = H + O_2(a) + M$	6.9(14)	0	–23000	[31]
34	$HO_2^{\cdot} + M = H + O_2(b) + M$	3.6(14)	0	–23000	″
35	$O_3 + M = O + O_2(a) + M$	4(14)	0	–22790	″
36	$O_3 + M = O + O_2(b) + M$	4(14)	0	–30384	″
37	$O + O_3 = O_2 + O_2(a)$	1.2(13)	0	–2300	[32]
38	$O + OH^{\cdot} = H + O_2(a)$	5.8(12)	0	–6224	[31]
39	$OH^{\cdot} + O_3 = HO_2^{\cdot} + O_2(a)$	3.2(11)	0	–1000	″
40	$OH^{\cdot} + O_3 = HO_2^{\cdot} + O_2(b)$	1.6 (11)	0	–1000	″
41	$H + HO_2^{\cdot} = H_2 + O_2(a)$	6(12)	0	–1518	″
42	$HO_2^{\cdot} + O_3 = OH^{\cdot} + O_2 + O_2(a)$	6.6(9)	0	–1000	″
43	$HO_2^{\cdot} + O_3 = OH^{\cdot} + O_2 + O_2(b)$	3.4(9)	0	–1000	″
44	$O_2 + O_2(a) = 2O_2$	1.4(4)	0.8	0	[32]
45	$O_3 + O_2(a) = O + 2O_2$	5.8(11)	0	–1564	″
46	$O_3 + O_2(b) = O + 2O_2$	1.1(13)	0	0	″
47	$H + O_2(a) + M = HO_2^{\cdot} + M$	1.5(15)	0	500	[31]
48	$H + O_2(b) + M = HO_2^{\cdot} + M$	1.5(15)	0	500	″
49	$O_2(a) + M = O + O + M$	5.4(18)	–1	–48008	″
50	$O_2(b) + M = O + O + M$	5.4(18)	–1	–40415	″
51	$O_2(a) + H_2O = OH^{\cdot} + HO_2^{\cdot}$	1.5(15)	0.5	–25209	″
52	$O_2(b) + H_2O = OH^{\cdot} + HO_2^{\cdot}$	1.5(15)	0.5	–17616	″
53	$O_2(a) + H_2O = O + H_2O_2$	3.4(10)	0.5	–34079	″
54	$O_2(b) + H_2O = O + H_2O_2$	3.4(10)	0.5	–27195	″
55	$O_2(a) + OH^{\cdot} = H + O_3$	4.4(7)	1.44	–27209	″
56	$O_2(b) + OH^{\cdot} = H + O_3$	4.4(7)	1.44	–19616	″
57	$O_2(a) + O_2(a) = O_2 + O_2(b)$	4.2(–4)	3.8	700	″
58	$O_2(a) + O = O + O_2$	4.2(8)	0	0	″
59	$O_2(a) + H = O + OH^{\cdot}$	1.1(14)	0	–3188	″
60	$O_2(b) + H = O + OH^{\cdot}$	1.1(14)	0	–1620	″
61	$O_2(a) + H_2 = OH^{\cdot} + OH^{\cdot}$	1.7(15)	0	–17906	″
62	$O_2(b) + H_2 = OH^{\cdot} + OH^{\cdot}$	1.7(15)	0	–14657	″
63	$O_2(a) + H_2 = H + HO_2^{\cdot}$	2.1(13)	0	–18216	″
64	$O_2(b) + H_2 = H + HO_2^{\cdot}$	2.1(13)	0	–11508	″
65	$O_2(a) + OH^{\cdot} = O + HO_2^{\cdot}$	1.3(13)	0	–17132	″
66	$O_2(b) + OH^{\cdot} = O + HO_2^{\cdot}$	1.3(13)	0	–10111	[31]
67	$O_2(a) + H_2O_2 = HO_2^{\cdot} + HO_2^{\cdot}$	3(13)	0	–10717	″
68	$O_2(b) + H_2O_2 = HO_2^{\cdot} + HO_2^{\cdot}$	3(13)	0	–4510	″
69	$O_2(a) + O_2 = O + O_3$	1.2(13)	0	–39732	″

Table 2. (Contd.)

No.	Reaction	A^+	m^+	E^+	Reference
70	$O_2(b) + O_2 = O + O_3$	1.2(13)	0	–32761	″
71	$O_2(a) + H = O_2 + H$	4.2(8)	0	0	″
72	$O_2(a) + O_3 = O_2 + O_3$	4.2(9)	0	0	″
73	$O_2(a) + H_2 = O_2 + H_2$	2.7(6)	0	0	″
74	$O_2(a) + O_2 = O_2 + O_2$	1(6)	0	0	″
75	$O_2(a) + OH^{\cdot} = O_2 + OH^{\cdot}$	3.4(6)	0	0	″
76	$O_2(a) + H_2O = O_2 + H_2O$	3.4(6)	0	0	″
77	$O_2(a) + HO_2^{\cdot} = O_2 + HO_2^{\cdot}$	3.4(6)	0	0	″
78	$O_2(a) + H_2O_2 = O_2 + H_2O_2$	3.4(6)	0	0	″
79	$O_2(a) + O_3 = O_2 + O_3$	2.4(9)	0	0	″
80	$O_2(b) + H = O_2(a) + H$	4.8(10)	0	0	″
81	$O_2(b) + O = O_2(a) + O$	4.8(10)	0	0	″
82	$O_2(b) + H_2 = O_2(a) + H_2$	4.9(11)	0	0	″
83	$O_2(b) + O_2 = O_2(a) + O_2$	2.8(7)	0	0	″
84	$O_2(b) + OH^{\cdot} = O_2(a) + OH^{\cdot}$	4(12)	0	0	″
85	$O_2(b) + H_2O = O_2(a) + H_2O$	4(12)	0	0	″
86	$O_2(b) + HO_2^{\cdot} = O_2(a) + HO_2^{\cdot}$	4(12)	0	0	″
87	$O_2(b) + H_2O_2 = O_2(a) + H_2O_2$	6(12)	0	0	″
88	$O_2(b) + O_3 = O_2(a) + O_3$	1.1(13)	0	0	″
89	$O_2(a) + O^- = O + O_2^-$	6(13)	0	0	[32]
90	$O_2(a) + O_4^+ = 2O_2 + O_2^+$	6(13)	0	0	″
91	$O_2(b) + O_4^+ = 2O_2 + O_2^+$	6(13)	0	0	″
92	$O_2(a) + O_4^- = 2O_2 + O_2^-$	6(13)	0	0	″
93	$O_2(b) + O_4^- = 2O_2 + O_2^-$	6(13)	0	0	″
94	$O_2(a) + O^- = O_3 + e$	1.8(14)	0	0	″
95	$O_2(b) + O^- = O + O_2 + e$	4.2(14)	0	0	″
96	$O_2(a) + O_2^- = 2O_2 + e$	1.2(14)	0	0	″
97	$O_2(b) + O_2^- = 2O_2 + e$ 32	2.2(14)	0	0	″
98	$2O_2 + O_2^+ = O_2 + O_4^+$	7.4(25)	–3.2	0	″
99	$O_2 + O_4^+ = 2O_2 + O_2^+$	1.6(28)	–4	–5030	″
100	$O_2^+ + O_2^- = 2O_2$	2.1(18)	–0.5	0	″
101	$O_2^+ + O_2^- = 2O + O_2$	6(16)	0	0	″
102	$O^- + O_2^+ = 3O$	6(16)	0	0	[32]
103	$O_2^+ + O_3^- = 2O + O_3$	6(16)	0	0	″
104	$O_2^- + O_4^+ = 3O_2$	6(16)	0	0	″
105	$O^- + O_4^+ = O + 2O_2$	6(16)	0	0	″
106	$O_3^- + O_4^+ = 2O_2 + O_3$	6(16)	0	0	″
107	$O^+ + O_2^- = O + O_2$	2.1(18)	–0.5	0	″
108	$O_2^+ + O_3^- = O_2 + O_3$	2.1(18)	–0.5	0	″

Table 2. (Contd.)

No.	Reaction	A^+	m^+	E^+	Reference
109	$O^+ + O_3^- = O + O_3$	2.1(18)	–0.5	0	″
110	$O^- + O_2^+ = O + O_2$	2.1(18)	–0.5	0	″
111	$O^- + O^+ = O + O$	2.1(18)	–0.5	0	″
112	$O_2 + O^+ = O + O_2^+$	2(13)	0	–0.00169	″
113	$O_3 + O^+ = O_2 + O_2^+$	6(13)	0	0	″
114	$O + O_4^+ = O_3 + O_2^+$	1.8(14)	0	0	″
115	$O_4^+ + H_2O = O_3H_2^+ + O_2$	9(14)	0	0	[37]
116	$H_2O^+ + H_2O = H_3O^+ + OH^{\cdot}$	1(15)	0	0	″
117	$H_2O^+ + O_2 = O_2^+ + H_2O$	2.6(14)	0	0	[41]
118	$O^+ + O_2 + O = O_2 + O_2^+$	3.6(18)	0	0	[32]
119	$2H_2 + H^+ = H_2 + H_3^+$	2(20)	–0.5	0	[33]
120	$2H_2 + H_3^+ = H_2 + H_5^+$	2.4(17)	0	0	″
121	$H_2 + H_2^+ = H + H_3^+$	1.3(15)	0	0	″
122	$H + H_2^+ = H_2 + H^+$	3.9(14)	0	0	″
123	$H_2 + H^+ = H + H_2^+$	1.5(15)	0	0	″
124	$H_2 + H_5^+ = 2H_2 + H_3^+$	2.4(11)	0	0	″
125	$2O_2 + O^- = O_2 + O_3^-$	1.2(20)	–1	0	[32]
126	$O_2 + O_3^- = 2O_2 + O^-$	9.8(23)	–2	18260	″
127	$O + O_3^- = O_3 + O^-$	2.7(14)	0	–12025	″
128	$O + O_2^- = O_2 + O^-$	2(14)	0	0	″
129	$O + O_4^- = 2O_2 + O^-$	1.8(14)	0	0	″
130	$O_3 + O_2^- = O_2 + O_3^-$	2.4(14)	0	0	″
131	$O_3 + O^- = O + O_3^-$	3.2(14)	0	0	[32]
132	$O_2 + O^- = O + O_2^-$	2.7(14)	0	–12025	″
133	$O_2 + O_3^- = O_3 + O_2^-$	4(14)	0	–18380	″
134	$O + O_3^- = O_2 + O_2^-$	1.9(14)	0	0	″
135	$O + O_4^- = O_2 + O_3^-$	2.4(14)	0	0	″
136	$H_2O + H^- = H_2 + OH^-$	2.3(15)	0	0	[37]
137	$O_2 + O_3^- + O_2^+ = O_3 + 2O_2$	1.1(29)	–2.5	0	[32]
138	$O_2 + O_3^- + O_2^+ = O_3 + O_2 + 2O$	1.1(29)	–2.5	0	″
139	$O_2 + O_2^- + O_2^+ = 2O_2 + 2O$	1.1(29)	–2.5	0	″
140	$O_2 + O_2^+ + O_2^- = 3O_2$	1.1(29)	–2.5	0	″
141	$O_2 + O^+ + O_2^- = O + 2O_2$	1.1(29)	–2.5	0	″
142	$O_2 + O^- + O_2^+ = O + 2O_2$	1.1(29)	–2.5	0	″
143	$O_2 + O^- + O^+ = 2O + O_2$	1.1(29)	–2.5	0	″
144	$O_2 + O^+ + O_2^- = O_2 + O_3$	1.1(29)	–2.5	0	″

Table 2. (Contd.)

No.	Reaction	A^+	m^+	E^+	Reference
145	$O_2 + O^- + O_2^+ = O_2 + O_3$	1.1(29)	–2.5	0	″
146	$O_2 + O^- + O^+ = 2O_2$	1.1(29)	–2.5	0	″
147	$H^+ + H^- = H(n = 2) + H$	4.8(11)	0.83	0	[33]
148	$H^+ + H^- = H(n = 3) + H$	1.9(18)	–0.5	0	″
149	$H_2^+ + H^- = H + H_2$	2.1(18)	–0.5	0	″
150	$H_3^+ + H^- = 2H_2$	2.1(18)	–0.5	0	″
151	$H_5^+ + H^- = 3H_2$	2.1(18)	–0.5	0	″
152	$O + O^- = O_2 + e$	3(14)	0	0	[32]
153	$O_2 + O^- = O_3 + e$	3(9)	0	0	″
154	$O + O_2^- = O_3 + e$	8.1(18)	–2	0	″
155	$O_2 + O_2^- = 2O_2 + e$	9.4(12)	0.5	–5590	″
156	$O_2 + O + O_2^- = O_3 + O_2 + e$	1.1(18)	0	0	″
157	$O^- + O_3 = 2O_2 + e$	1.8(14)	0	0	[40]
158	$O_3^- + O_2 = O_3 + O_2 + e$	6(9)	0	0	[38]
159	$O_3^- + O_3 = 3O_2 + e$	6(11)	0	0	″
160	$O + O_3^- = 2O_2 + e$	1.8(14)	0	0	[32]
161	$H + H^- = H_2 + e$	7.8(14)	0	0	[33]
162	$OH^- + O = HO_2^{\bullet} + e$	1.2(14)	0	0	[37]
163	$OH^- + H = H_2O + e$	1.1(15)	0	0	[37]
164	$H^- + H = H_2 + e$	7.8(14)	0	0	″
165	$H^- + O_2 = HO_2^{\bullet} + e$	7.2(14)	0	0	″
166	$O_2 + H_2O + e = O_2^- + H_2O$	3.6(17)	0	0	[39]
167	$O_3 + e = O + O_2^-$	6(14)	0	0	[32]
168	$O_3 + e = O_2 + O^-$	6(12)	0	0	″
169	$O + O_2 + e = O^- + O_2$	3.6(16)	0	0	″
170	$O + O_2 + e = O + O_2^-$	3.6(16)	0	0	″
171	$O_2 + O_3 + e = O_2 + O_3^-$	1.5(25)	–2	0	″
172	$O_3H_2^+ + H_2O = H_3O^+ + OH^{\bullet} + O_2$	1.8(14)	0	0	[38]
173	$O_2^- + H_3O^+ = H_2O + O_2 + H$	1.2(18)	0	0	″
174	$O_3^- + O_3H_2^+ = O_2 + H_2O + O_3$	4.2(18)	–0.5	0	″
175	$O_3^- + H_3O^+ = O_2 + H_2O + OH^{\bullet}$	4.2(18)	–0.5	0	″
176	$OH^- + H_3O^+ = H_2O + H_2O$	4.2(18)	–0.5	0	″
177	$OH^- + O_3H_2^+ = H_2O + OH^{\bullet} + O_2$	4.2(18)	–0.5	0	″
178	$H^- + H_3O^+ = H_2O + H_2$	4.2(18)	–0.5	0	″

Table 3. Reaction rate constants depending on electron temperature T_e, $k^+ = A^+ T_e^{m_e^+} \exp(E_e^+/T_e)$

No.	Reaction	A^+	m_e^+	E_e^+	Reference
179	$2e + H^+ = H(n) + e$	k_{179}			[33]
180	$e + H_2^+ = H + H$	1.8(19)	–0.5	–1	″
181	$e + H_3^+ = 3H$	1.8(19)	–0.5	–1	″
182	$e + H_5^+ = H + 2H_2$	2.9(17)	–0.5	0	″
183	$O + e = O^+ + 2e$	4.8(10)	–1	–13.617	[32]
184	$O_2^+ + e = 2O$	3.1(15)	–1	0	″
185	$O_4^+ + e = 2O_2$	1.3(17)	0	0	″
186	$O_2^+ + 2e = O_2 + e$	2.7(21)	–4.5	0	″
187	$O^+ + 2e = O + e$	2.7(21)	–4.5	0	″
188	$O_2 + e + O_2^+ = 2O_2$	2.4(17)	–2.5	0	″
189	$O_2 + e + O^+ = O + O_2$	2.4(17)	–2.5	0	″
190	$H_2O + e = H + OH^{\bullet} + e$	3.2(15)	0.5	–8	[34]
191	$H_2O + e = OH^+ + H + 2e$	2.8(15)	0.5	–18	″
192	$H_2O + e = H_2O^+ + 2e$	8.4(15)	0.5	–15	″
193	$H_2O + e = OH^{\bullet} + H^-$	5.5(14)	–1	–6.5	″
194	$H_2O + e = H_2 + O^-$	2.9(14)	–1	–8.6	″
195	$H_2 + e = 2H + e$	2(16)	0.5	–8.8	[35]
196	$H_2 + e = 2e + H_2^+$	1.2(16)	0.5	–15.42	[33]
197	$H_2 + e = H + H^-$	4.8(10)	–1	–3.75	″
198	$H + e = 2e + H^+$	5.2(15)	0.5	–13.597	″
199	$2e + H_2^+ = 2H + e$	3.2(21)	–4.5	0	″
200	$2e + H_3^+ = H + H_2 + e$	3.2(21)	–4.5	0	″
201	$2e + H_5^+ = H + 2H_2 + e$	3.2(21)	–4.5	0	″
202	$e + H^- = H + 2e$	1.2(17)	1.5	–1	″
203	$e + O^- = O + 2e$	2.4(16)	0	0	[35]
204	$O_2 + e = 2e + O_2^+$	7.8(15)	0.5	–12.2	[32]

Note: $k_{179} = \dfrac{2.3 \times 10^{21} n^2}{T_e^3 (e_n^{2.33} + 4.38 e_n^{1.72} + 1.32 e_n)}$, where $e_n = \dfrac{I_H}{n^2 T_e}$ and I_H is the ionization potential of the hydrogen atom (eV).

Table 4. Reaction rate constants depending on the reduced strength of the electric field θ, $k^+ = A^+\exp(E_\theta^+/\theta)$

No.	Reaction	A^+	E_θ^+	Reference
205	$O_2 + e = O_2(a) + e$	k_{205}		[32]
206	$O_2 + e = O_2(b) + e$	k_{206}		″
207	$2O_2 + e = O_2 + O_2^-$	k_{207}		″
208	$O_2 + e = 2O + e$	3.1(16)	–32.236	″
209	$O_2 + e = O + O^-$	3(14)	–28.32	″
210	$O_3 + e = O + O_2 + e$	3.1(17)	–32.236	″
211	$H_2 + e = H + 2e + H^+$	9.5(14)	–64.7	[33]

Note: $k_{205} = \begin{cases} 3.8\times10^{13}\exp(-0.8059/\theta),\ \theta<4 \\ 6.0\times10^{14}\exp(-11.973/\theta),\ \theta>4; \end{cases}$ $k_{206} = \begin{cases} 3.8\times10^{12}\exp(-1.658/\theta),\ \theta<3 \\ 1.9\times10^{14}\exp(-13.82/\theta),\ \theta>3; \end{cases}$ $k_{207} = (17.03 - 0.906\theta)\times10^{16}$.

almost constant, reactive atoms and radicals build up, determining the combustion dynamics. Later on, the gas temperature rises sharply and the system passes to a new thermodynamic state. The induction period under these conditions is τ_{in} = 1 ms. The induction period was calculated as a function of the composition of the H_2–O_2 mixture at various temperatures. The ignition delay turned out to depend on both the hydrogen-to-oxygen ratio and gas temperature. As the temperature is raised, the induction period shortens, no matter what the mixture composition. At any temperature, the ignition delay lengthens as the hydrogen-to-oxygen ratio either increases or decreases relative to the stoichiometric composition (ϕ = 1).

The ignition of the hydrogen–oxygen mixture by low-temperature gas-discharge plasma was analyzed using a model taking into account the dissociation of molecules and the formation of active radicals and charged species. Considering that the gas temperature

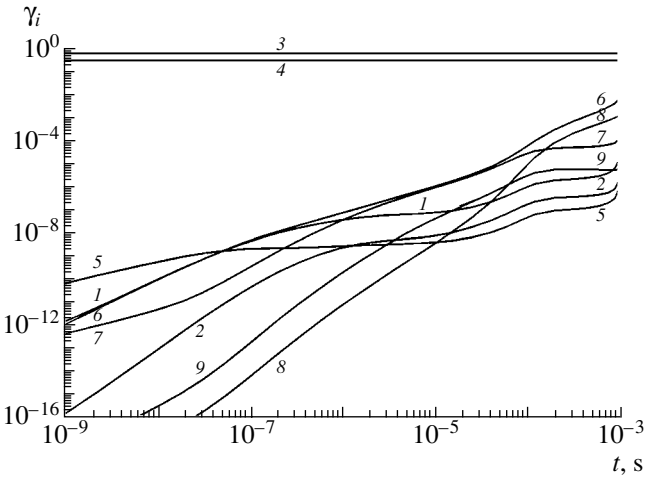

Fig. 1. Time dependence of component mole fractions (γ_i) for the autoignition of the stoichiometric (2 : 1) H_2–O_2 mixture with an instantaneous temperature rise to T_0 = 900 K at $P_0 = 10^5$ Pa: (*1*) H, (*2*) O, (*3*) H_2, (*4*) O_2, (*5*) OH, (*6*) H_2O, (*7*) HO_2, (*8*) H_2O_2, and (*9*) O_3.

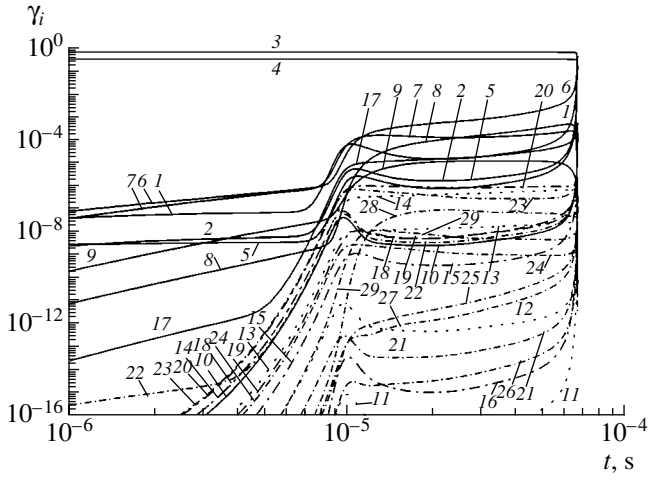

Fig. 2. Time dependence of component mole fractions (γ_i) for the gas discharge–induced ignition of the stoichiometric (2 : 1) H_2–O_2 mixture with an instantaneous temperature rise to T_0 = 900 K at $P_0 = 10^5$ Pa and T_e = 1.4 eV: (*1*) H, (*2*) O, (*3*) H_2, (*4*) O_2, (*5*) OH, (*6*) H_2O, (*7*) HO_2, (*8*) H_2O_2, (*9*) O_3, (*10*) e, (*11*) H^+, (*12*) H_2^+, (*13*) H_3^+, (*14*) H_5^+, (*15*) O^-, (*16*) O^+, (*17*) $O_2(a^1\Delta_g)$, (*18*) O_2^-, (*19*) O_3^-, (*20*) O_4^-, (*21*) H^-, (*22*) $O_2(b^1\Sigma_g^+)$, (*23*) O_2^+, (*24*) O_4^+, (*25*) OH^+, (*26*) H_2O^+, (*27*) OH^-, (*28*) H_3O^+, and (*29*) $O_3H_2^+$.

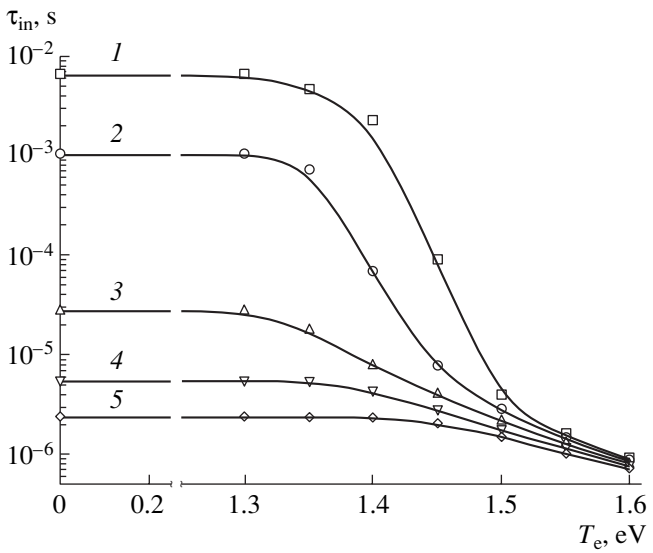

Fig. 3. Effect of the gas discharge on the induction period for the ignition of the stoichiometric (2 : 1) H_2–O_2 mixture at $P_0 = 10^5$ Pa with an instantaneous temperature rise to T_0 = (*1*) 800, (*2*) 900, (*3*) 1000, (*4*) 1100, and (*5*) 1200 K.

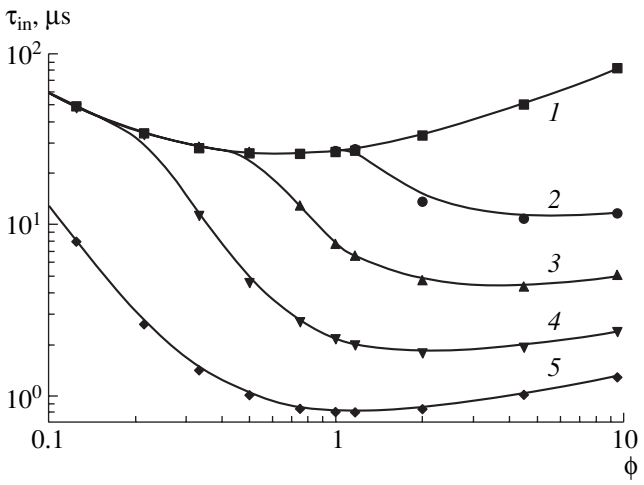

Fig. 4. Induction period as a function of the hydrogen content of the H_2–O_2 mixture at $P_0 = 10^5$ Pa, $T_0 = 1000$ K, and T_e = (*1*) 0, (*2*) 1.3, (*3*) 1.4, (*4*) 1.5, and (*5*) 1.6 eV.

under microwave discharge conditions increases at a rate of about 10^2 K/μs, the process was simulated under the assumption that, after the electric field is switched on, the gas temperature rises instantaneously to some initial value T_0. The energy dissipation and the diffusion of active species into the environment was neglected. Calculations were made for an initial H_2–O_2 pressure of $P_0 = 0.1$ MPa, initial gas temperatures of $T_0 = 800$–1200 K, and electron temperatures of $T_e = 0.1$–1.6 eV.

Figure 2 illustrates the development of nonthermal ignition under the action of low-temperature plasma at $T_e = 1.4$ eV. Applying a discharge reduces τ_{in} to 67 μs and changes the ignition mechanism. The formation of free radicals and active species is markedly accelerated by the discharge, and charged species participate in the formation of active radicals (excitation, dissociation, and electron-impact ionization take place). The ionization frequency increases sharply as the electron temperature (i.e., the reduced strength of the electric field) is raised. At 900 K, the avalanche delay time decreases from ~200 μs at $T_e = 1.35$ eV to ~0.5 μs at $T_e = 1.6$ eV. As the avalanche develops, not only charged species but also radicals and active atoms build up. At the avalanche development stage, the concentrations of the metastable molecules $O_2(a^1\Delta_g)$ and $O_2(b^1\Sigma_g^+)$, H and O atoms, and radicals increases by one order of magnitude at $T_e = 1.35$ eV and by 5–6 orders of magnitude at $T_e = 1.6$ eV. Of course, this shortens the induction period markedly. The concentrations of charged species come to equilibrium through recharging ion collisions and electron attachment and detachment. At the stage preceding the ignition of the oxygen–hydrogen mixture, the most abundant positive ions in the discharge are H_5^+ and O_2^+ and the dominating negative ion is O_4^-.

Figure 3 illustrates the effect of a gas discharge on the ignition delay for a stoichiometric (2 : 1) H_2–O_2 mixture at $P_0 = 10^5$ Pa for instantaneous temperature jumps to various T_0 values. Clearly, the delay time in the ignition induced by nonequilibrium low-temperature plasma decreases by several orders of magnitude as

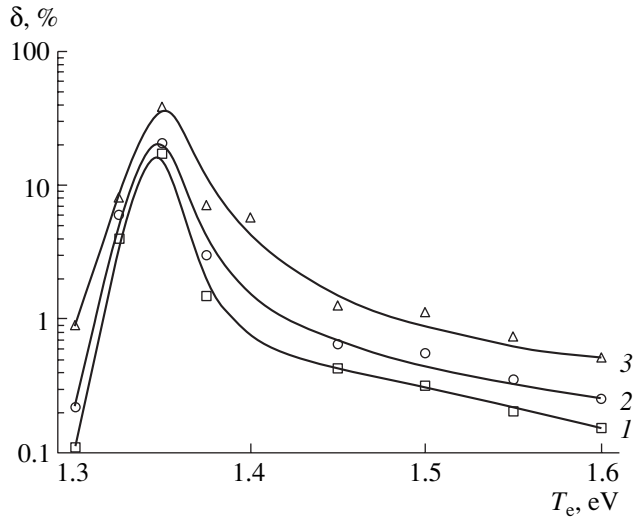

Fig. 5. Error in the induction period calculated using the reduced kinetic networks (*1*) RKN1, (*2*) RKN2, and (*3*) RKN3 versus electron temperature at $P_0 = 10^5$ Pa and $T_0 = 900$ K.

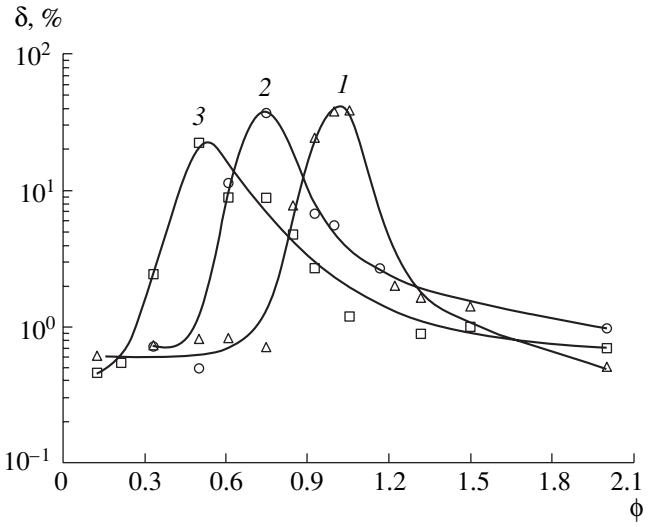

Fig. 6. Error in the induction period calculated using the reduced kinetic network RKN3 versus the composition of the H_2–O_2 mixture at $P_0 = 10^5$ Pa, $T_0 = 900$ K, and T_e = (*1*) 1.35, (*2*) 1.4, and (*3*) 1.45 eV.

the electron temperature increases. Furthermore, calculations have demonstrated that, as the hydrogen content of the mixture is increased above the stoichiometric value, the gas discharge causes a progressively greater shortening effect on the ignition delay (Fig. 4). At the same time, low-temperature plasma exerts a much weaker effect on lean mixtures. This result is indirect evidence that, at the early stages of the ignition of the H_2–O_2 mixture induced by gas-discharge plasma, electrons form mainly by the ionization of hydrogen molecules. At later stages, the mixture components undergo excitation, dissociation, and ionization by colliding with electrons. Electron attachment and detachment, recharging collisions, and the recombination of charged species take place simultaneously. All these processes lead to the nonequilibrium formation of active species (O and H atoms and $OH^{\cdot}$ radicals), which participate in branched-chain reactions to intensify the chain combustion of hydrogen.

Using the basic kinetic network and four reduced networks, we calculated the induction period for gas discharge–induced ignition at various temperatures, pressures, mixture compositions, and electron temperatures. The first reduced kinetic network (RKN1) includes 29 components and 168 reactions, the second (RKN2) includes 23 components and 113 reactions, the third (RKN3) includes 21 components and 89 reactions, and the fourth (RKN4) includes 22 components and 81 reactions. At $P_0 = 10^5$ Pa, $T_0 = 900$ K, and various T_e values, RKN1 provides a good description for the ignition of the hydrogen–oxygen mixture (Fig. 5). Use of this reaction network instead of the unreduced network generally introduces an error no greater than 10% in the induction period. The largest error is observed for $T_e = 1.35$ eV. If other conditions, for example, a lower initial temperature is set in the calculations, the error will be greater. For $P_0 = 10^5$ Pa, $T_0 = 800$ K, and $T_e = 1.4$ eV, RKN4 leads to an error greater than 100%. At $P_0 = 10^4$ Pa, $T_0 = 700$ K, and $T_e = 1.1$ eV, even RKN1 leads to an error of 42%. For RKN3, the error in the induction period as a function of the composition of

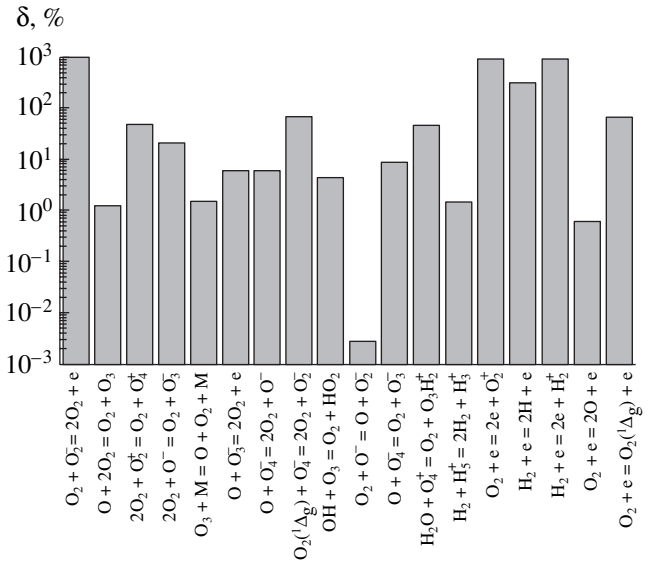

Fig. 7. Sensitivity of the kinetic model to reactions quickening ignition as calculated using RKN3 for $P_0 = 10^5$ Pa, $T_0 =$ 900 K, and $T_e = 1.4$ eV.

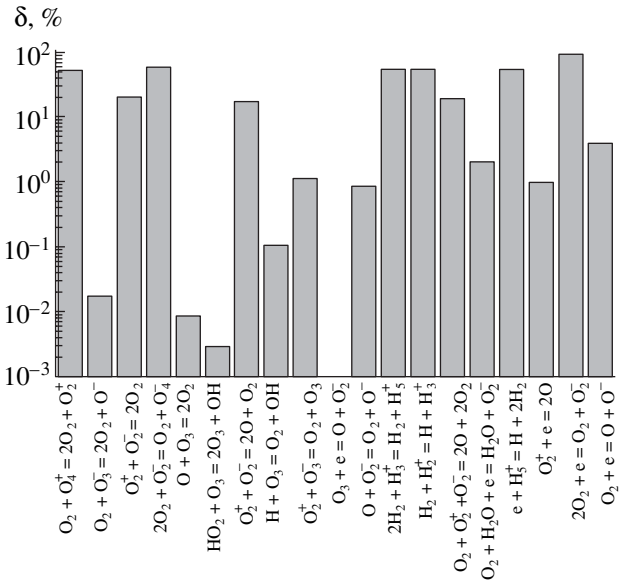

Fig. 8. Sensitivity of the kinetic model to reactions retarding ignition as calculated using RKN3 for $P_0 = 10^5$ Pa, $T_0 =$ 900 K, and $T_e = 1.4$ eV.

the H_2–O_2 mixture at $P_0 = 10^5$ Pa, $T_0 = 900$ K, and various T_e values is plotted in Fig. 6. Clearly, the error in τ_{in} depends strongly on process conditions. These results demonstrate that the basic kinetic network should be reduced in a specific way in each particular case.

In order to determine the contributions from mixture components and main reaction channels to the acceleration or deceleration of the branched-chain reactions involved in the ignition of hydrogen–oxygen mixtures, we analyzed the sensitivity of the kinetic model to various reactions occurring during the nonthermal ignition induced by lower-temperature plasma. Calculations based on RKN3 were carried out for a variety of conditions. The results of these calculations are presented in Figs. 7 and 8. These figures show the contributions made by the accelerating reactions (Fig. 7) and decelerating reactions (Fig. 8) to the ignition induced by low-temperature plasma.

Thus, we have simulated the initiation of the nonthermal ignition in the hydrogen–oxygen system, taking into account the active radicals and excited and charged species produced by nonequilibrium gas-discharge plasma. The nonthermal effect of the gas discharge on the ignition event is most pronounced at low gas temperatures, at which the autoignition time is long. When reducing the basic kinetic network, it is necessary to perform additional studies to check whether the network chosen is adequate to the given set of conditions.

ACKNOWLEDGMENTS

This work was supported by the Russian Foundation for Basic Research (grant nos. 02-02-17116 and 05-02-16532) and by EOARD grant no. 2248r.

REFERENCES

1. Semenov, N.N., *Tsepnye reaktsii* (Chain Reactions), Moscow: Nauka, 1986.
2. Lewis, B. and Von Elbe, G., *Combustion, Flames, and Explosions of Gases*, New York: Academic, 1961.
3. Coffee, T.R., *Combust. Flame*, 1984, vol. 55, no. 2, p. 161.
4. Frenklach, M. and Bornside, D.E., *Combust. Flame*, 1984, vol. 56, no. 1, p. 1.
5. Seery, D.J. and Bowman, C.T., *Combust. Flame*, 1970, vol. 14, p. 37.
6. Azatyan, V.V., *Doctoral (Chem.) Dissertation*, Moscow: Inst. of Chemical Physics, 1978.
7. Dautov, N.G. and Starik, A.M., *Kinet. Katal.*, 1997, vol. 38, no. 2, p. 207.
8. Starik, A.M., Titova, N.S., and Yanovskii, L.S., *Kinet. Katal.*, 1999, vol. 40, no. 1, p. 11.
9. Semenov, N.N., *O nekotorykh problemakh khimicheskoi kinetiki i reaktsionnoi sposobnosti* (Some Problems of Chemical Kinetics and Reactivity), Moscow: Akad. Nauk SSSR, 1958.
10. Nalbandyan, A.B., *Zh. Fiz. Khim.*, 1946, vol. 20, p. 1259.
11. *International Space Planes and Hypersonic System and Technologies Conf., Workshop on Weakly Ionized Gases: Proc. AIAA*, Colorado, 1997; Norfolk, 1998, 1999; Anaheim, 2001; Reno, 2002, 2003, 2004.
12. *The International Workshops on Magneto- and Plasma Aerodynamics for Aerospace Applications*, Moscow, 1999, 2000, 2001, 2002, 2003.
13. Bozhenkov, S.A., Starikovskaya, S.M., and Starikovskii, A.Y., *Combust. Flame*, 2003, vol. 133, p. 133.
14. Seleznev, A.A., Aleinikov, A.Yu., and Yaroshenko, V.V., *Khim. Fiz.*, 1999, vol. 18, no. 5, p. 65.
15. Basevich, V.Ya. and Belyaev, A.A., *Khim. Fiz.*, 1989, vol. 8, no. 8, p. 1124.
16. Tanoff, M.A., Smooke, M.D., Teets, K.E., and Sell, J.A., *Combust. Flame*, 1995, vol. 103, no. 4, p. 253.
17. Ma, J.X., Alexander, D.R., and Poulain, D.E., *Combust. Flame*, 1998, vol. 112, no. 4, p. 492.
18. Morsy, M.H., Ko, Y.S., and Chung, S.H., *Combust. Flame*, 1999, vol. 119, no. 4, p. 492.
19. Ershov, A.P., Surkont, O.S., Timofeev, I.B., *et al.*, *Teplofiz. Vys. Temp.*, 2004, vol. 42, no. 5, p. 669.
20. Zarin, A.S., Kuzovnikov, A.A., and Shibkov, V.M., *Svobodno lokalizovannyi SVCh razryad v vozdukhe* (Unconfined Localized Microwave Discharge in Air), Moscow: Neft i Gaz, 1996.
21. Shibkov, V.M., Vinogradov, D.A., Voskanyan, A.V., *et al.*, *Vestn. Mosk. Univ., Ser. 3: Fiz.*, 2000, vol. 41, no. 6, p. 64.
22. Shibkov, V.M., Aleksandrov, A.F., Ershov, A.P., *et al.*, *Vestn. Mosk. Univ., Ser. 3: Fiz.*, 2004, vol. 45, no. 5, p. 67.
23. Shibkov, V.M., Aleksandrov, A.F., Ershov, A.P., *et al.*, *Fiz. Plazmy*, 2005, vol. 31, no. 9, p. 857.
24. Shibkov, V.M., Chernikov, A.V., Ershov, A.P., *et al.*, *AIAA Pap.*, 2004, nos. 2004-0513, 2004-0838.
25. Raizer, Yu.P., *Fizika gazovogo razryada* (Gas Discharge Physics), Moscow: Nauka, 1987.
26. Shibkov, V.M., *Teplofiz. Vys. Temp.*, 1996, vol. 34, no. 4, p. 525.
27. Lodinev, V.V., Shibkov, V.M., and Shibkova, L.V., *Vestn. Mosk. Univ., Ser. 3: Fiz.*, 1996, vol. 37, no. 2, p. 29.
28. Shibkov, V.M., *Teplofiz. Vys. Temp.*, 1997, vol. 35, no. 5, p. 693.
29. Shibkov, V.M., *Teplofiz. Vys. Temp.*, 1997, vol. 35, no. 6, p. 871.
30. Zlobina, Yu.V., Shibkov, V.M., and Shibkova, L.V., *Fiz. Plazmy*, 1998, vol. 24, no. 7, p. 667.
31. Starik, A.M. and Titova, N.S., *Kinet. Katal.*, 2003, vol. 44, no. 1, p. 35.
32. Kostinsky, A.Y., Matveev, A.A., and Silakov, V.P., *Preprint of General Physics Inst., Academy of Sciences of the USSR*, Moscow, 1990, no. 87.
33. Matveev, A.A. and Silakov, V.P., *Preprint of General Physics Inst., Russian Academy of Sciences*, Moscow, 1994, no. 8.
34. Bychkov, V.L. and Gordeev, O.A., *Khim. Fiz.*, 1992, vol. 11, no. 8, p. 1064.

35. Slovetskii, D.I., *Khimiya plazmy* (Plasma Chemistry), Smirnov, B.M., Ed., Moscow: Atomizdat, 1974.
36. Samoilovich, V.G., Gibalov, V.I., and Kozlov, K.V., *Fizicheskaya khimiya bar'ernogo razryada* (Physical Chemistry of the Barrier Discharge), Moscow: Mosk. Gos. Univ., 1989.
37. McEven, M. and Phillips, L., *Chemistry of the Atmosphere*, London: Arnold, 1975.
38. Akishev, Yu.S., Deryugin, A.A., Karal'nik, V.B., *et al.*, *Fiz. Plazmy*, 1994, vol. 20, no. 6, p. 571.
39. Aleksandrov, N.L., *Usp. Fiz. Nauk*, 1988, vol. 154, no. 2, p. 147.
40. Steinfeld, J.I., Adler-Golden, S.M., and Gallagher, J.W., *J. Phys. Chem. Ref. Data*, 1987, vol. 16, no. 4, p. 911.
41. Person, J.C. and Ham, D.O., *Radiat. Phys. Chem.*, 1988, vol. 31, nos. 1–3, p. 1.
42. *Termodinamicheskie svoistva individual'nykh veshchestv: Spravochnik* (Thermodynamic Properties of Individual Compounds: A Handbook), Glushko, V.P., Ed., Moscow: Nauka, 1978, vol. 1; 1979, vol. 2.